Distribution Category:
Magnetic Fusion Energy-
Fusion Systems (UC-420)

ANL/FPP/TM-227

ANL/FPP/TM--227

DE88 016957

Argonne National Laboratory
9700 South Cass Avenue
Argonne, Illinois 60439

LIQUID METAL FLOW IN A LARGE-RADIUS ELBOW *WITH A UNIFORM MAGNETIC FIELD*

T. J. Moon
and
J. S. Walker

July 1988

Work supported by

Office of Fusion Energy
U.S. Department of Energy
Under Contract W-31-109-ENG-38

CONTENTS

LIST OF FIGURES

LIQUID METAL FLOW IN A LARGE-RADIUS ELBOW WITH A UNIFORM MAGNETIC FIELD

T. J. Moon and J. S. Walker

ABSTRACT

This paper treats the liquid-metal flow in an elbow between two straight, rectangular ducts. There is a uniform magnetic field in the plane of the elbow. The duct has thin, electrically conducting walls. The Hartmann number and the interaction parameter are assumed to be large, while the magnetic Reynolds number is assumed to be small. Solutions for the velocity at each cross section of the elbow and for the pressure drop due to three-dimensional effects are presented.

1. INTRODUCTION

Since 1967, a series of papers have presented asymptotic solutions for three-dimensional liquid-metal duct flows in strong magnetic fields. Many of the pre-1984 papers are discussed by Walker [1]. The present paper represents an extension of this literature in two ways: (1) elimination of the assumption of symmetry about a plane perpendicular to the magnetic field and (2) a more physically realistic asymptotic analysis for flows in ducts with thin metal walls.

Here we treat the flow in an elbow lying in the plane of a uniform magnetic field, $B_o\hat{y}$ where $\hat{y}$ is a unit vector. The rectangular duct has one pair of plane, parallel walls (sides) at $z = \pm 1$, where (x,y,z) are the cartesian coordinates normalized by L, which is half the distance between the sides. The other pair of walls (top and bottom) are: (1) plane and perpendicular to the magnetic field at $y = 0$, and $y = a$, for $x < 0$, (2) arcs of concentric cylinders with centers at $x = 0$, $y = R_o$, and with dimensionless radii = R_o and $R_o - a$, for $0 < x < R_o \sin\theta_e$, and (3) plane and at an angle $(90^\circ - \theta_e)$ to the magnetic field for $x > R_o \sin\theta_e$. The flow in this duct is not symmetric about any y = constant plane. Walker [2] presents an asymptotic analysis for the corresponding symmetric problem, i.e., for the same uniform magnetic field and for the same plane, parallel sides, but for symmetrically diverging or converging top and bottom at $y = \pm f(x)$. The present analysis assumes a symmetry about the $z = 0$ plane for computational convenience. Walker [3,4] has eliminated the assumption of symmetry about a plane parallel to the magnetic field for circular pipes and rectangular ducts, respectively.

In addition to the elimination of the symmetry assumption, the result for the present elbow have practical implications for the design of liquid-lithium-cooled "blankets" for magnetic confinement fusion reactors. Several proposed designs [5] involve elbows from straight ducts which are nearly perpendicular to the local magnetic field to straight ducts which are nearly parallel to it. For a toroidal fusion reactor (tokamak), a poloidal-toroidal elbow corresponds approximately to $\theta_e = 85^\circ$, since the strength of the poloidal magnetic field is roughly one-tenth that of the toroidal field.

For liquid metal MHD duct flows, an important parameter is the wall conductance ratio, $c = \sigma_w t/\sigma L$, where t is the thickness of the duct walls, and σ_w and σ are the electrical conductivities of the walls and liquid metal, respectively. The value of c is small for many practical applications. For liquid lithium fusion blankets with thin stainless steel walls, the range of c is 0.01 to 0.1. Until recently, asymptotic solutions

for small c were considered appropriate for these applications. These solutions involve asymptotic expansions in powers of $c^{1/2}$ and predict certain characteristic surfaces which are parallel to the magnetic field lines [6]. They also predict that $v_\perp = O(c^{1/2} v_{||})$ and $j_\perp = O(c^{1/2} j_{||})$, where $\underset{\sim}{v}$ and $\underset{\sim}{j}$ are the velocity and electric current density, and the subscripts $_\perp$ and $_{||}$ denote the components perpendicular and parallel to the characteristic surfaces. To leading order, the flow and electric current must follow the characteristic surfaces. For the present elbow for $0 \leq x \leq R_o \sin\theta_e$, the asymptotic solution for small c predicts that the total flow is carried by high-velocity sheet jets in the thin viscous layers adjacent to the sides and that the rest of the fluid in the elbow is essentially stagnant. The dimensionless velocity in the side layers is $O(M^{1/2})$, and the side layer thickness is $O(M^{-1/2})$, where $M = B_o L(\sigma/\rho\nu)^{1/2}$ is the Hartmann number, while ρ and ν are the liquid metal's density and kinematic viscosity. For a typical fusion blanket, $M = 10^4 - 10^5$. The velocity outside the side layers is $O(c^{1/2})$, which is considered negligible in this small c asymptotic solution.

Results of recent experiments at Argonne National Laboratory for a different three-dimensional flow in a rectangular duct with $M = 6 \times 10^3$ and $c = 0.07$ differ radically from the predictions of the asymptotic analysis for small c. In the three-dimensional flow region of these experiments, the velocity near the sides increases and that near the centerline decreases, but the flow is far from the predicted stagnant core with all the flow in high-velocity side-layer jets. In retrospect, the fault of the small c asymptotic analyses and their characteristic surfaces is evident. The ratios $j_\perp/j_{||}$ and $v_\perp/v_{||}$ are actually proportional to $\lambda_1 c^{1/2}$, where λ_1 is the first eigenvalue for a set of equations which depend on the duct geometry. Typical values for λ_1 are 10.64 for a circular duct[6] and 2.25 for a square duct, (for a square duct with the same wall conductance ratio, $c \ll 1$, on all four walls, transcendental equation is $\tan(2\lambda_n) = 2\lambda_n$ and first eigenvalue is $\lambda_1 = 2.24671$ {Abramowitz & Stegun, p. 224}), so that $\lambda_1 c^{1/2}$ is comparable to one, even for $c = 0.01$. Therefore $j_\perp$ and $v_\perp$ are always comparable to $j_{||}$ and $v_{||}$, respectively, so that the flow and electric current are not constrained to follow the characteristic surfaces predicted by the small asymptotic analyses.

There are two ways to obtain more realistic predictions for three-dimensional MHD duct flows with strong magnetic fields and with $c = 0.01$-0.1. The first way is to discard the asymptotic analysis for small c entirely and to treat c as an O(1) parameter. This approach leads to coupled partial differential equations which generally require numerical analysis[7]. This arbitrary c approach is necessary for small radius elbows,

e.g., R_o = a, and a future paper will present numerical results for sharp, right-angle elbows.

The second way to obtain more realistic predictions involves an improved small c asymptotic analysis for flows with relatively weak three-dimensional effects. In many important applications, the transition in geometry and/or magnetic field strength which is responsible for the three-dimensional disturbance occurs over a duct length L_{3D} which is much larger than L. For such gradual transitions,

$$\gamma = c^{1/2} L_{3D}/L$$

is an important parameter. In an asymptotic solution for small c, with the constraint that γ = O(1), i.e., that $L_{3D} = \gamma\, c^{-1/2}\, L >> L$, there are no characteristic surfaces guiding the flow and current, and there are no large stagnant regions. The error in this improved asymptotic treatment of weak three-dimensional effects is comparable to $\lambda_1 c^{1/2} L/L_{3D}$, which is small if L_{3D}/L is large.

This improved small c approach has been applied to a straight duct with a non-uniform transverse magnetic field whose strength changes from B_o to αB_o over a duct length of L_{3D}[8]. In recent experiments at Argonne National Laboratory, velocities, pressures and electric potentials were measured in a straight, rectangular duct with c = 0.07 near the end of a magnet, i.e., for α = 0. Taking L_{3D} to be the axial duct length for the magnetic field strength to change from $0.9B_o$ to $0.1B_o$, L_{3D} = 6.2L and γ = 1.64 for these experiments. For this end-of-magnet problem, we could expect an error in the improved small c approach equal to $\lambda_1 c^{1/2} L/L_{3D}$ = 9.5%. The experimental results and the predictions from both the arbitrary c numerical analysis and the improved small c asymptotic analysis will be presented in a future paper.

The present paper applies the improved small c approach with O(1) γ to elbows with large radii. In particular, $L_{3D} = R_o L$, so that $\gamma = R_o c^{1/2}$ is considered to be a fixed parameter as $c \to 0$. In §2, the problem is formulated and the core solution for a general geometry is presented. In §3, the sides and adjacent side layers are treated for the general geometry. In § 4, results are presented for an elbow whose top and bottom are concentric circular arcs. Some conclusions are presented in §5.

2. PROBLEM FORMULATION

The applied magnetic field is produced by an external magnet while the induced magnetic field is produced by the electric currents in the liquid metal and duct walls. The ratio of the induced to applied magnetic fields is $R_m c^{1/2}$, where

$$R_m = \mu\sigma U_o L$$

is the magnetic Reynolds number. Here μ is the liquid metal's magnetic permeability and U_o is the characteristic liquid-metal velocity. For a typical fusion reactor blanket, $R_m = 10^{-1}$ and $c = 10^{-2}$ [5], so that the induced magnetic field can be neglected. For the present problem the applied magnetic field is uniform, i.e., $\underset{\sim}{B} = B_o \hat{\underset{\sim}{y}}$, where $\hat{\underset{\sim}{y}}$ is a unit vector.

The ratio of the electromagnetic (EM) body force to the inertial "force" is the interaction parameter,

$$N = \frac{\sigma B_o^2 L}{\rho U_o}$$

For a typical fusion reactor blanket, $N = 10^3$-10^5 [5]. Therefore, inertial effects can be neglected except possibly in the boundary layers adjacent to the sides, which are parallel to the magnetic field. There are large velocities inside these side layers, and the inertial "force" may be locally comparable to the EM body force.

The square root of the ratio of the EM body force to the viscous force is the Hartmann number,

$$M = B_o L (\sigma/\rho\nu)^{1/2}$$

For a typical blanket, $M = 10^3 - 10^5$ [5], so that viscous effects are confined to boundary layers adjacent to the walls. The subregions of the flow are shown in Figure 1. The inviscid, inertialess core region (c) is separated from the top and bottom by the viscous Hartmann layers (h) with $O(M^{-1})$ thickness and from the sides by the side layers (S). The thickness δ and structure of the side layers depend on the relationship between the large parameters N and M.

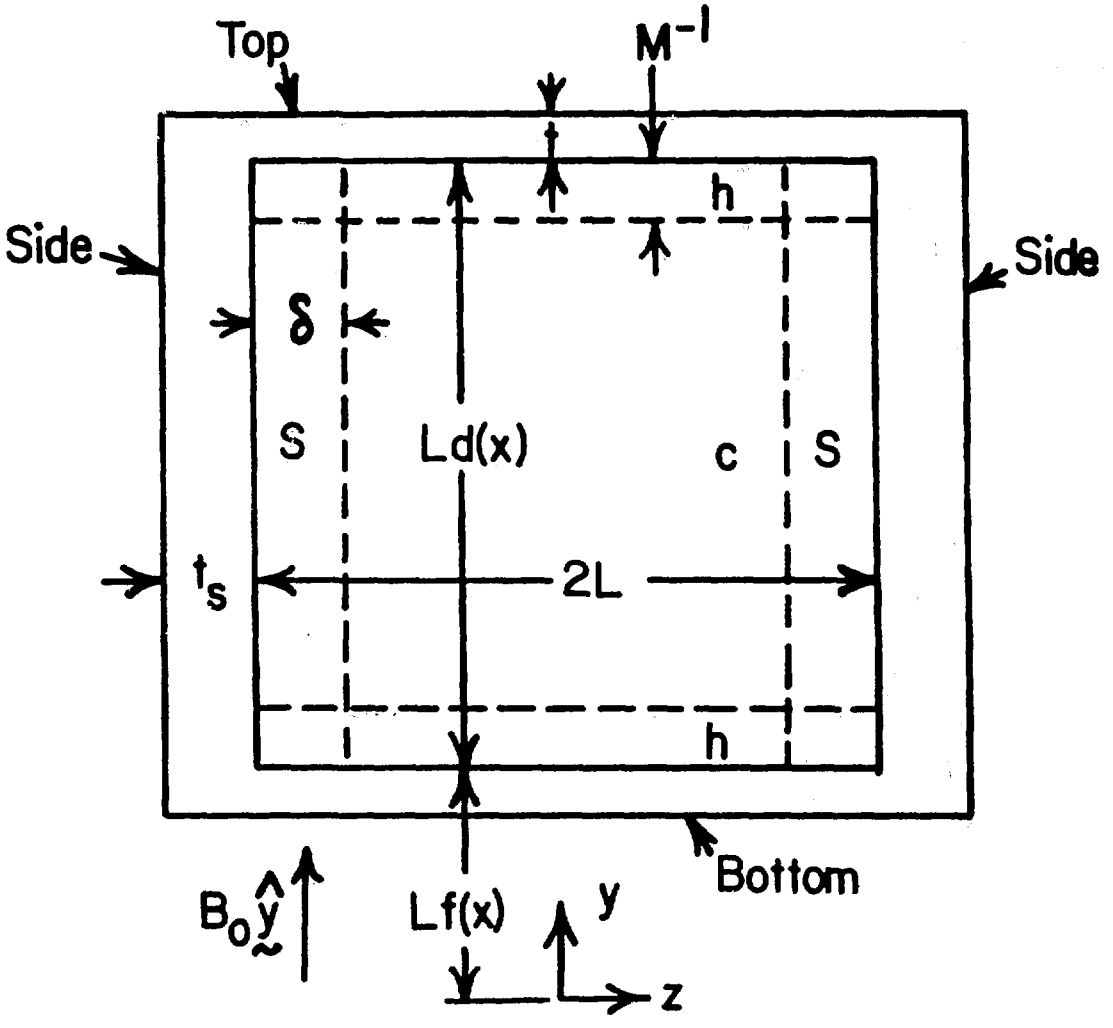

FIGURE 1. CROSS SECTION OF THE DUCT
SHOWING THE SUBREGIONS OF THE FLOW FOR M >> 1.

The dimensionless governing equations for steady, incompressible flow in a uniform magnetic field are

$$N^{-1} (\underset{\sim}{v}^* \cdot \underset{\sim}{\nabla}) \underset{\sim}{v}^* = - \underset{\sim}{\nabla} p^* + \underset{\sim}{j}^* \times \hat{y} + M^{-2} \nabla^2 \underset{\sim}{v}^*, \tag{1a}$$

$$\underset{\sim}{j}^* = -\underset{\sim}{\nabla} \phi^* + \underset{\sim}{v}^* \times \hat{y}^*, \qquad \underset{\sim}{\nabla} \cdot \underset{\sim}{v}^* = 0, \qquad \underset{\sim}{\nabla} \cdot \underset{\sim}{j}^* = 0 \tag{1b-d}$$

Here $\underset{\sim}{v}^*$, p^*, $\underset{\sim}{j}^*$ and ϕ^* are the velocity, pressure, electric current density and electric potential function, which are normalized by U_o, $\sigma U_o B_o^2 L$, $\sigma U_o B_o$, and $U_o B_o L$, respectively. The boundary conditions at the inside surface of each wall are that $\underset{\sim}{v}^* = 0$ and that ϕ^* and j^*_n are continuous between the wall and liquid metal. Here $j^*_n = \underset{\sim}{j}^* \cdot \hat{\underset{\sim}{n}}$, where $\hat{\underset{\sim}{n}}$ is a unit normal to the wall surface, into the liquid. If the outside surfaces of the top and bottom are electrically insulated and if $t \ll L$, then the electric potential is continuous through the thickness of the top or bottom and the liquid-metal variables must satisfy the thin conducting wall condition

$$j^*_n = c \left[\frac{\partial^2 \phi^*}{\partial s^2} + \frac{\partial^2 \phi^*}{\partial z^2}\right], \text{ at } y = f(x), \text{ or at } y = f(x) + d(x) \tag{2}$$

This condition neglects terms which are $O(t^2/L^2)$ compared to those retained [6]. Here s is the tangential distance along the top or bottom in the $z = 0$ plane, as shown in Figure 2. The same assumptions for the sides lead to the condition

$$j^*_z = \mp c_s \left[\frac{\partial^2 \phi^*}{\partial x^2} + \frac{\partial^2 \phi^*}{\partial y^2}\right], \text{ at } z = \pm 1, \tag{3}$$

where $c_s = \sigma_w t_s / \sigma L$ is the wall conductance ratio for each side with thickness $t_s \ll L$.

The flow is symmetric about the $z = 0$ plane, so that u^*, v^*, j^*_z and p^* are even functions of z, while w^*, j^*_x, j^*_y and ϕ^* are odd functions of z. Here u^*, v^*, and w^* are the x, y and z components of $\underset{\sim}{v}^*$. We need only treat the flow for $0 \leq z \leq 1$. Upstream, the top and bottom become perpendicular to the magnetic field and are separated by a distance aL. We choose the average axial velocity at an upstream cross section as U_o, so that the dimensionless velocity satisfies a volume flux condition

$$\int_f^{f+d} \int_0^1 u^*(x,y,z)\, dz\, dy = a \tag{4}$$

at each x = constant section.

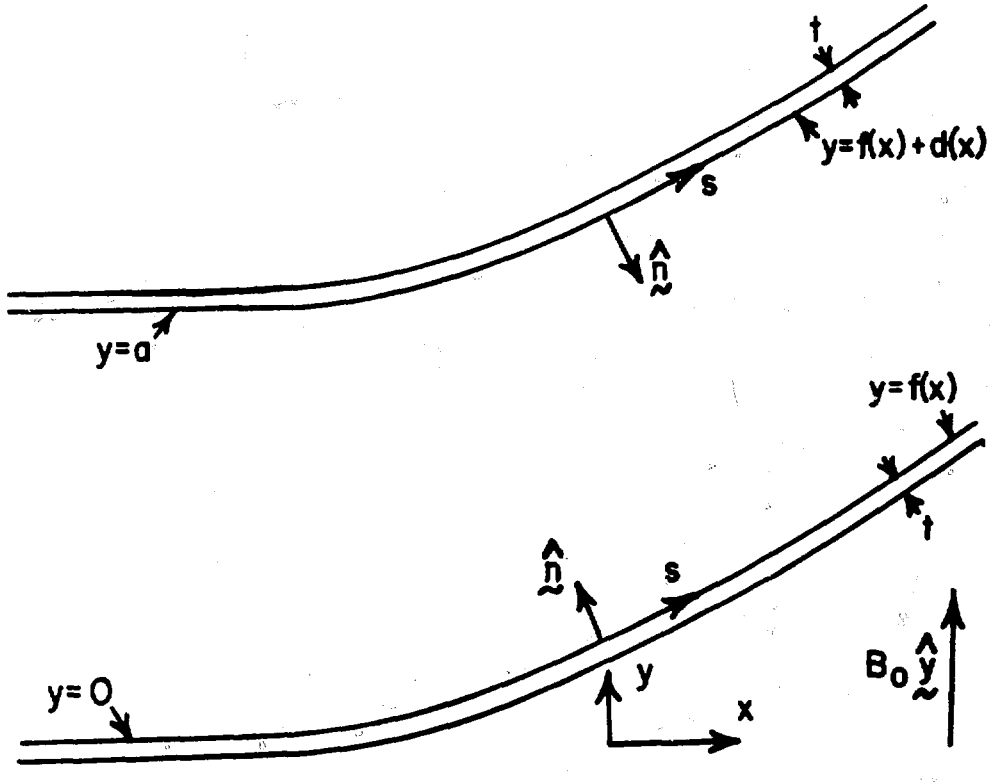

FIGURE 2. LONGITUDINAL SECTION OF THE DUCT AT z = 0, SHOWING s, THE TANGENTIAL DISTANCE ALONG THE INSIDE SURFACE OF THE TOP OR BOTTOM.

The Hartmann layers satisfy the no-slip condition at the top and bottom and match the core or side-layer velocity, provided the latter satisfies

$$v^*_n = 0, \quad \text{at } y = f(x), \quad \text{or at } y = f(x) + d(x), \tag{5}$$

neglecting $O(M^{-1})$ terms. The jump in j^*_n or ϕ^* across a Hartmann layer is at most $O(M^{-1})$, so that the condition (2) can be applied to the core or side-layer variables if $c >> M^{-1}$ [9].

Since $c = 10^{-2}$ and $M = N = 10^{-3} - 10^{-5}$, (1) we neglect the viscous and inertial terms in the momentum equation (1a) except in the side layers, (2) we seek asymptotic solutions of the boundary value problem (1-5) in powers of the small parameter c, where $c_s = \beta c$ and β is an O(1) parameter, and (3) we keep

$$\gamma = R_o c^{1/2}$$

as an O(1) parameter, where R_o is the characteristic dimensionless radius of curvature of the bottom, normalized with L. If the elbow has an $O(c^{-1/2})$ radius of curvature and reaches an O(1) slope, then f(x) becomes large, namely $O(c^{-1/2})$, but d(x) remains O(1) as long as the duct's axis does not become parallel to the magnetic field. With the large radius of curvature, the values of the variables at a given position in the x = constant cross sections of duct vary gradually with x. Two steps are needed to represent this gradual variation between cross sections. The first step is to introduce

$$Y = y - f(x)$$

as a local y coordinate which varies from 0 at the bottom to d(x) at the top. The x derivative of any variable as a function of (x, Y, z) is small, namely $O(c^{1/2})$. Therefore, the second step is to compress the axial coordinate by introducing

$$X = c^{1/2}x, \quad f = c^{-1/2} F(X), \quad d = D(X)$$

The variables have O(1) relative changes with O(1) variations of X; i.e., the derivatives with respect to X, Y and z are independent of the small parameter c. The top and bottom both reach O(1) slopes, but the difference between their slopes at a given x =

constant cross section is $O(\epsilon^{1/2})$, so that they are almost parallel at each x = constant section.

In the inviscid, inertialess core, u^*, v^* and ϕ^* are O(1); w^*, j^*_x, j^*_y and p^* are $O(\epsilon^{1/2})$; j^*_z is $O(\epsilon)$ [2]. Therefore we introduce the following asymptotic expansions for the core variables:

$$u^* = u + \epsilon^{1/2} U + O(\epsilon),$$

$$v^* = v + \epsilon^{1/2} V + O(\epsilon),$$

$$w^* = \epsilon^{1/2} w + O(\epsilon),$$

$$\phi^* = \phi + \epsilon^{1/2} \Phi + O(\epsilon),$$

$$j^*_x = \epsilon^{1/2} j_x + \epsilon J_x + O(\epsilon^{3/2}),$$

$$j^*_y = \epsilon^{1/2} j_y + \epsilon J_y + O(\epsilon^{3/2}),$$

$$j^*_z = \epsilon j_z + O(\epsilon^{3/2}),$$

$$p^* = \epsilon^{1/2} p + O(\epsilon),$$

Here, lower case and capital letters denote the coefficient functions in the first and second terms in the asymptotic expansions for the starred variables. We are only interested in the first term in each expansion. When the equations (1) and the boundary conditions (2,5) are applied to the leading order terms, they give the solutions

$$j_x = \frac{\partial p}{\partial z}, \qquad j_y = F' j_x, \qquad j_z = -\frac{\partial p}{\partial X}, \qquad u = \frac{\partial \phi}{\partial z}, \tag{6a-d}$$

$$v = F' u, \qquad w = -\frac{\partial \phi}{\partial X} - G \frac{\partial p}{\partial z} \tag{6e,f}$$

Here $p(X,z)$ and $\phi(X,z)$ are completely arbitrary functions. In order to determine these functions, we must determine some of the second terms in the asymptotic expansions,

namely those denoted by capital letters above. When we apply some of the equations (1) and the boundary conditons (2,5) to the second terms, we obtain the solutions for the second terms involving two new unknown functions of X and z. We also obtain two coupled ordinary differential equations with respect to z which govern p(X,z) and ϕ(X,z) with the following solutions:

$$p = P + A\,[\cosh(r\,z) - \cosh(r)], \tag{6g}$$

$$\phi = \left(D/2 \right)^{1/2} G^{1/4} A \sinh(r\,z), \tag{6h}$$

where

$$G = 1 + (F')^2, \qquad r = D' (2\,D)^{-1/2} G^{-3/4}, \tag{6i,j}$$

and a prime denotes differentiation of F(X) or D(X). The integration functions A(X) and P(X) are determined when the side-layer and side-wall problems are treated in the next section. The core perturbations, denoted by capital letters, are not presented here because their only role is to determine the ordinary differential equations governing ϕ(X,z) and p(X,z).

The O(1) tangential velocity which is parallel to the top and bottom is

$$v_s(X,z) = G^{-1/2} (u + F'\,v) = \frac{1}{2} D' A \cosh(rz), \tag{7}$$

for all Y, while the velocity parallel to the normal to the bottom is $O(\epsilon^{1/2})$ throughout. Plots of the core velocity and pressure for a circular elbow are presented in § 4.

3. SIDE-LAYER AND SIDE-WALL PROBLEMS

At z = 1 in the core, the $O(\epsilon)$ $j_z = -P'(X) > 0$. For an O(1) ΔX, this represents an $O(\epsilon^{1/2})$ total electric current equal to $-(\Delta X)\,D\,P'$. This current leaves the core, flows across the side layer and enters the side at z = 1. Half of this current flows up or down in the side and enters the top at Y = D, z = 1 or the bottom at Y = 0, z = 1. The O(1) transverse electric current density in the top or bottom is

$$j_{zt} = -\frac{1}{2}\left(\frac{\sigma_w}{\sigma}\right) D' G^{-1/2} A \cosh(r z) \tag{8}$$

The total axial electric currents in the side layer and in the side are $O(\delta c^{1/2})$ and $O(c^{3/2})$, respectively, and these are too small to divert any of the $O(c^{1/2})$ total current leaving the core at $z = 1$. All of this $O(c^{1/2})$ current must enter the top and bottom in the same ΔX and become j_{zt} at $z = 1$. Therefore, conservation of electric current gives

$$P' = -D' D^{-1} A \cosh(r) \tag{9}$$

for the pressure gradient in the core at $z = 1$.

Since c_s is comparable to c, the electric currents flowing up and down in the side imply that the O(1) electric potential function in the side, $\Phi(X,Y)$, must vary with Y. However, the O(1) core potential (6h) is independent of Y, so that there is a jump in the O(1) electric potential across the side layer. Since j_z is small in the side layer, the y and z components of Ohm's law (1b) become

$$j_{yS} = -\frac{\partial \phi_S}{\partial y}, \qquad u_S = \delta^{-1}\frac{\partial \phi_S}{\partial \zeta}, \quad \zeta = \delta^{-1}(z-1) \tag{10a-c}$$

where the subscript S denotes a side-layer variable and ζ is the stretched side-layer coordinate. The result (10a) and the conservation of current equation (1d) imply that

$$j_z = -c P'(X) + \delta j_{zS}(X,Y,\zeta) \tag{11}$$

When we introduce the large velocity (10b) and the small electric current density (11) into the x component of the momentum equation (1a), this equation determines the side-layer thickness δ. If the inertial or viscous terms balance the EM body force associated with j_{zS}, then

$$\delta_I = N^{-1/3} c^{1/6} \quad \text{or} \quad \delta_V = M^{1/2},$$

respectively. The c enters δ_I because $(\underline{v} \cdot \underline{\nabla})\underline{v} = \delta^{-2} c^{1/2}$, due to the gradual variations between cross sections. If $\delta_V >> \delta_I$, i.e., if $N >> M^{3/2} c^{1/2}$, then the side layer is a purely viscous layer with an $O(M^{-1/2})$ thickness and an $O(M^{1/2})$ tangential velocity

parallel to the top and bottom. If $\delta_I >> \delta_V$, i.e., if $N << M^{3/2} c^{1/2}$, then there is an inertial layer with a thickness δ_I and an $O(\delta_I^{-1})$ tangential velocity. This inertial side layer is separated from the side by a thinner viscous layer with an $O(M^{-1/2})$ thickness and an $O(\delta_I^{-1})$ tangential velocity. This viscous inner layer is needed to satisfy the no-slip condition at z = 1.

We can determine (a) the remaining integration function A(X) in the core solution (6), (b) the side electric potential $\Phi(X,Y)$ and (c) the total O(1) volume flux through a ΔY of the side layer in any X = constant cross section from the equation (10b), namely

$$q_S(X,Y) = \delta \int_{-\infty}^{0} u_S \, d\zeta = \Phi(X,Y) - \phi(X,1), \tag{12}$$

without treating the side-layer problem, provided two conditions are satisfied. The thin conducting wall condition (3) and the transverse side-layer current (11) give

$$\beta G \frac{\partial^2 \Phi}{\partial Y^2} = P'(X) - \frac{\delta}{c} j_{zS}(X,Y,0) \tag{13}$$

The first condition is that $\delta << c$, so that the last term in the equation (13) can be ignored. The O(c) transverse current density from the core flows unchanged across the side layer. This condition requires that

$$c >> M^{1/2}, \text{ and } c >> N^{-2/5} \tag{14a,b}$$

The second condition is obtained by introducing the core solution (6d) and the side-layer volume flux (12) into the total volume flux condition (4) to get

$$\int_0^{D(X)} \Phi(X,Y) \, dY = a \tag{15}$$

If Φ satisfies this condition, then we are guaranteed (a) that the equations (1) have a solution for either the purely viscous side layer or for the inertial outer layer and viscous inner layer, (b) that this solution can match the side potential Φ, can match the core solution (6) and can satisfy the relevant boundary conditions at the side and at the top and bottom, and (c) that the total volume flux in the side layer and core equals a.

While the O(1) electric potential has a jump across the side layer, it is continuous in the walls at the corners. Therefore the solution of equation (13) is

$$\Phi(X,Y) = \phi(X,1) - \frac{Y\ (D - Y)\ P'}{2\ \beta\ G} \tag{16}$$

The electric current flowing from the side to the top and bottom is conserved at the corners if P' is given by the solution (9). The volume flux condition (15) and the solutions (6h, 9,16) give

$$A(X) = a[\ D\ (D/2)^{1/2}\ G^{1/4} \sinh(r) + \frac{D'\ D^2}{12\ \beta\ G}\ \cosh(r)\ ]^{-1} \tag{17}$$

The side layer is a high-velocity sheet jet adjacent to the wall which is parallel to the magnetic field. The volume flux inside this layer has a parabolic distribution with zero flux at the top and bottom where the electric potential is continuous and with a maximum flux at Y = D/2. The relationship between the fractions of the total volume flux carried by the O(1) velocity in the core and the $O(\delta^{-1})$ velocity in the side layer corresponds to the relationship between the two terms in the expression (17), where the first and second terms represent the core and side layer, respectively. The volume flux in the side layer relative to that in the core varies as β^{-1} and D' coth (r). As $\beta = c_s/c$ increases, the side-layer volume flux decreases. For large values of D', r is large and the side layer flux increases linearly as D' increases. For small values of D', r is small and the side layer volume flux is nearly independent of D'. These statements are true for a viscous side layer with $\delta = \delta_V$, for an inertial side layer with $\delta = \delta_I$, or for an inertial-viscous layer when δ_V and δ_I are comparable.

4. RESULTS FOR A CIRCULAR ARC ELBOW

Here we treat two straight, constant-area, rectangular ducts which are connected by an elbow whose top and bottom are concentric circular arcs, as shown in Figure 3. After the $\epsilon^{1/2}$ rescaling presented in § 2,

$$F = \gamma - (\gamma^2 - X^2)^{1/2}, \quad D = \gamma\ a\ (\gamma^2 - X^2)^{-1/2}, \tag{18a,b}$$

for $0 \le X \le X_e = \gamma \sin \theta_e$, where the expression (18b) neglects terms which are $O(\epsilon^{1/2})$.

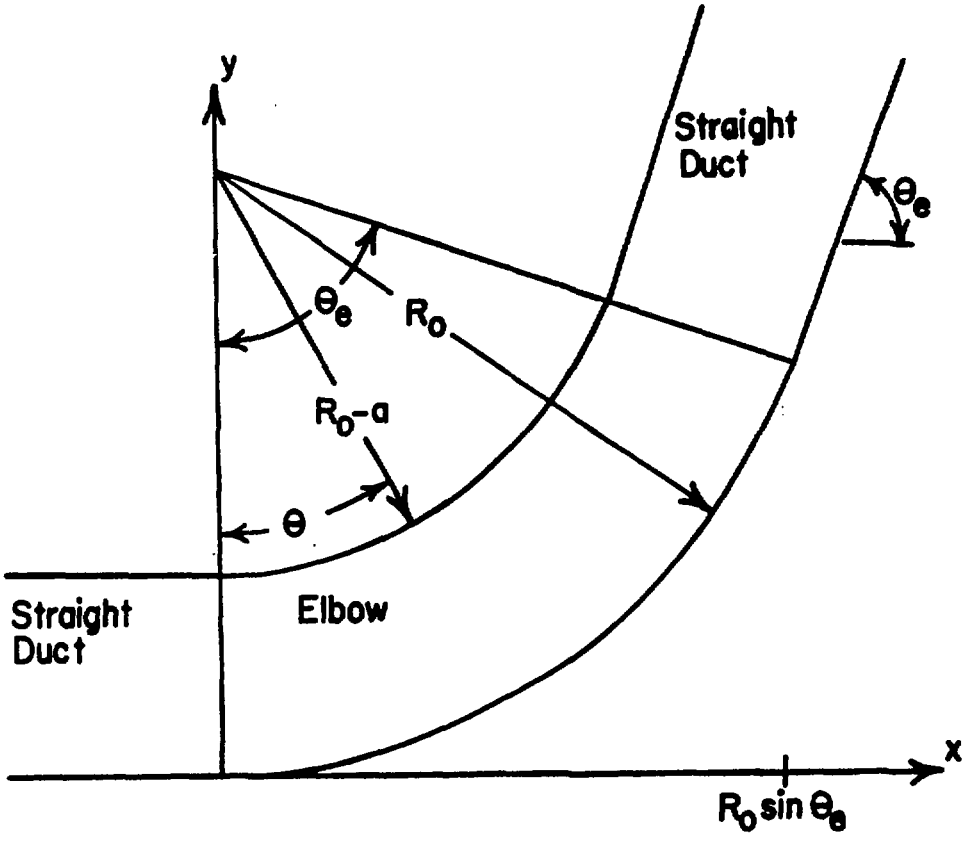

FIGURE 3. LONGITUDINAL SECTION OF A CIRCULAR ARC ELBOW BETWEEN TWO STRAIGHT DUCTS

The solutions (6,7,9,16,17) are local solutions for each X = constant cross section because the assumption that $\gamma = R_o c^{1/2} = O(1)$ leads to the neglect of axial derivatives. We consider an elbow from $\theta = 0$ to $\theta = \theta_e = 85°$. The solution in any elbow with $\theta_e < 85°$ is given by the flow in the appropriate part of the 85° elbow. The core velocity v_s parallel to the top and bottom is given by the solution (7) and is plotted in Figure 4 for $a = \beta = 1$ and for various values of γ and θ. At $X = \theta = 0$, the core velocity is uniform. As $X = \gamma \sin \theta$ increases, the core velocity near $z = 0$ decreases, while that near $z = \pm 1$ increases. The migration of the flow toward the sides and the increase in the fraction of the flow carried by the side layers continue to the exit at X_e because D' increases from 0 at $X = 0$ to a $\gamma^{-1} \tan \theta_e \sec^2 \theta_e$ at $X = X_e$. As $x \to \infty$, the flow becomes the fully developed flow in a straight rectangular duct with a transverse magnetic field equal to $B_o \cos \theta_e$. The axial component of the magnetic field $B_o \sin \theta_e$ has no effect on the fully developed flow. There is a transition region with O(1) axial derivatives near the junction at θ_e. To treat this region we introduce

$$x^* = x - R_o \sin \theta_e.$$

Derivatives with respect to x*, y and z are all O(1) in the transition region. The transition region consists of three subregions: (a) for $-\infty < x^* < -a \sin \theta_e$, both the top and bottom are circular arcs with large radii; (b) for $-\sin \theta_e < x^* < 0$, the top is straight, but the bottom is still a circular arc; (c) for $0 < x^* < \infty$, both the top and bottom are straight. In each subregion, the three basic variables are the $O(c^{1/2})$ core pressure $p(x^*,z)$, the O(1) core potential $\phi(x^*,z)$ and the O(1) side potential $\Phi(x^*,y)$. These three variables are governed by three coupled, second-order, elliptic partial differential equations. The equations are different for each subregion, and the three subregions are linked by the conditions that each variable and its axial derivative are continuous at $x^* = -a \sin \theta_e$ and at $x^* = 0$. Velocity and pressure profiles for a similar transition region are presented by Walker[8], while the analysis for this similar transition region is presented in an Argonne National Laboratory Technical Memo[10]. For the present transition region: (a) as $x^* \to -\infty$, the solution approaches the solution (6, 7, 9, 16, 17) at $X = X_e$, and (b) as $x^* \to \infty$, the solution approaches the appropriate fully developed flow solution. In fact, the deviation from the fully developed flow decays exponentially as x* increases from 0, so that the flow becomes fully developed in a distance comparable to L after the end of the elbow.

There is no transition region at X = 0 because D' = 0 here and the solution (6,7,9,16,17) for D' = 0 is the locally fully developed flow solution with a uniform core velocity and no axial electric currents. If we replace the upstream straight duct with one which has a -5° slope and which joins the circular-arc elbow at $\theta = -5°$, then we have a 90° elbow from a duct at $\theta = -5°$ to a duct at $\theta = 85°$. This coincides with a poloidal-to-toroidal elbow in a tokamak blanket because there is a toroidal magnetic field B_T and a poloidal magnetic field $B_P \tilde{=} 0.1\ B_T$. For this modified duct, there is a weak transition region at $\theta = -5°$ and the solution for $-5° \leq \theta \leq 0$ is given by the present solution for $0 \leq \theta \leq 5°$.

Comparison of Figures 4a and b indicates that the non-uniformity of the core velocity increases as the elbow radius $R_0 = \gamma\ c^{-1/2}$ decreases. For c = 0.01, γ = 0.25 and 1 corresponds to the radius of the bottom equal to 1.25 and 5 times the distance between the sides, respectively. For a square duct (a = 2) and for c = 0.01, a sharp corner in the top corresponds to γ = 0.2. However, for such a sharp elbow, axial derivatives are not negligible as assumed here. In order to keep both R_0 and γ as O(1) parameters, c must be treated as an O(1) parameter whose value is specified in the problem. This leads to boundary value problems which require numerical solutions[7]. A future paper will present numerical results for sharp elbows in the plane of a uniform magnetic field. At the other extreme of elbows with very large radii, the flow remains nearly fully developed throughout the elbow, as indicated by the results in Figure 4c for large values of γ.

From the equations (6a,b,g) the axial core current parallel to the top and bottom is

$$j_s = G^{-1/2}\ (j_x + F'\ j_y) = G^{1/2}\ A\ r \sinh (rz)$$

This represents a current in the ± x direction for $z \gtrless 0$, and these axial currents produce a transverse pressure variation so that p (X,0) < p (X, ± 1) = P(X). This is the case for flow from a duct which is perpendicular to the magnetic field to a duct which is nearly parallel to it. For flow from a nearly parallel duct to a perpendicular duct, i.e., for flow in the -x direction in Figure 3, the transverse pressure variation is reversed and the centerline pressure is greater than the side pressure. Since inertial effects play no role in this problem, the flow in the -x direction is given by changing the sign of all variables. The magnitudes of the axial currents and of the transverse pressure difference

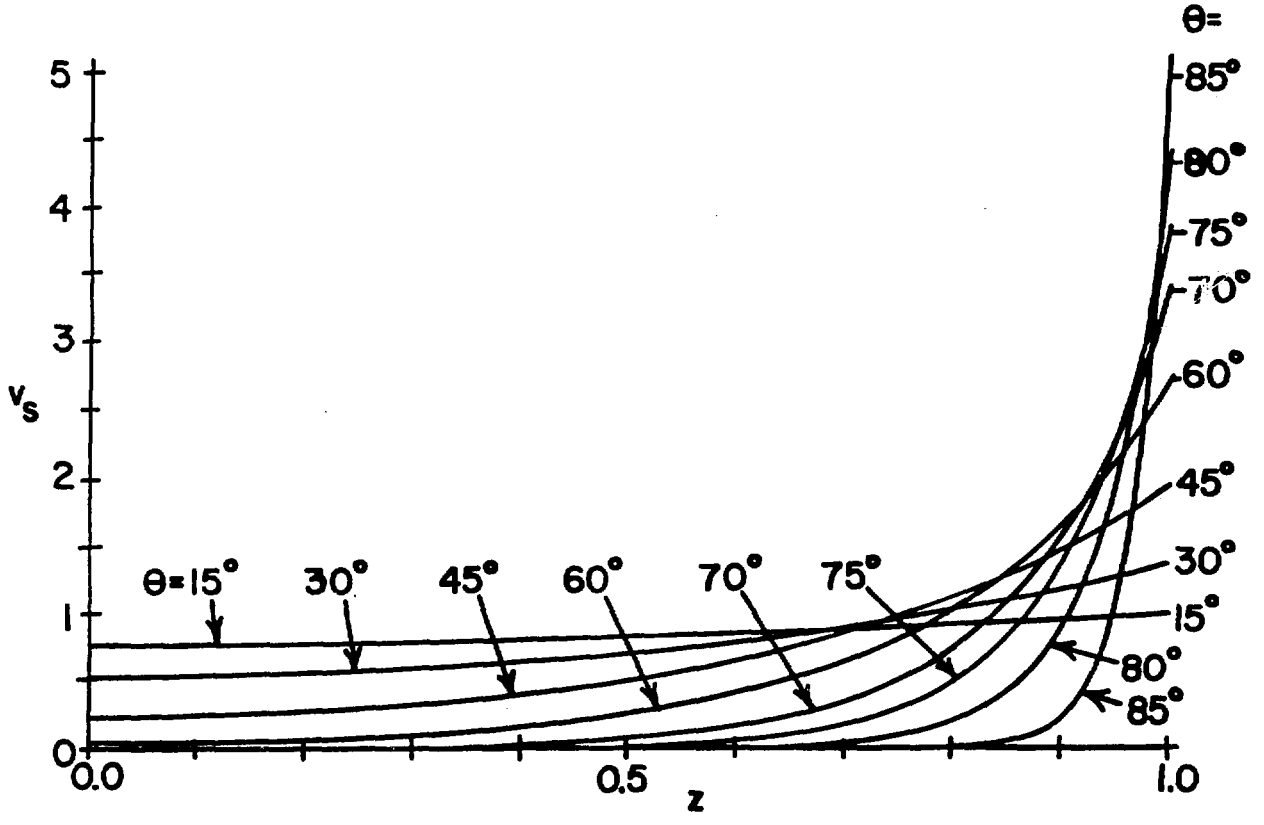

FIGURE 4a. THE CORE VELOCITY V_S PARALLEL TO THE TOP AND BOTTOM FOR $a = \beta = 1$. ($\gamma = 0.25$ and various θ).

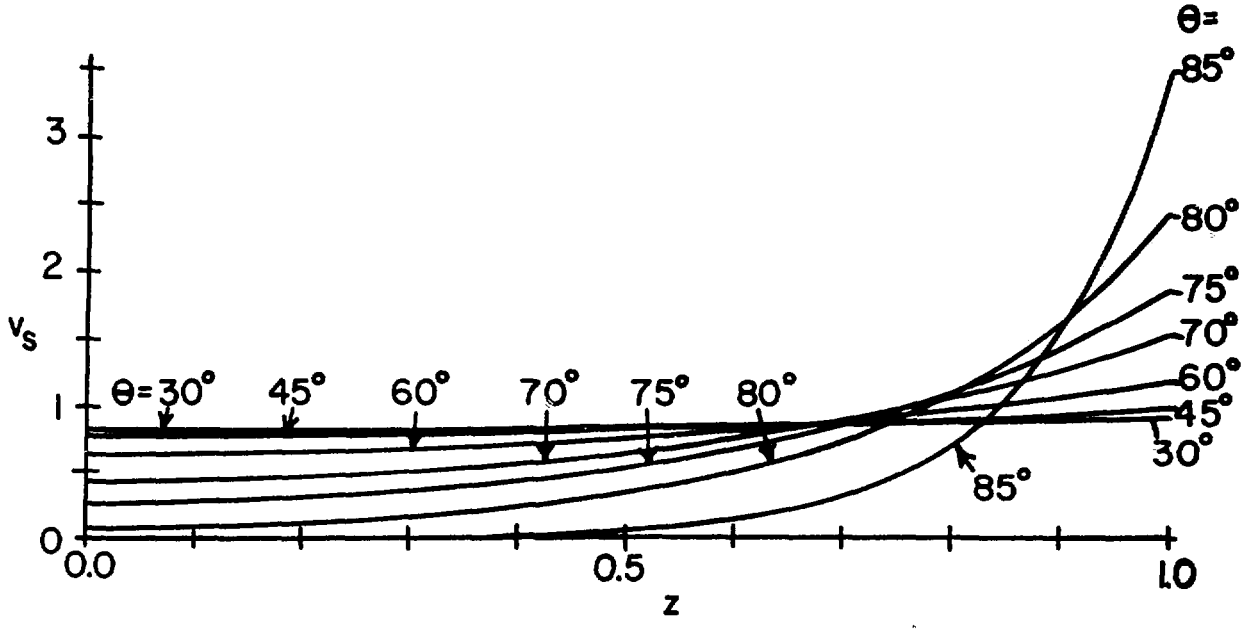

FIGURE 4b. THE CORE VELOCITY V_s PARALLEL TO THE TOP AND BOTTOM FOR a = β = 1. (γ = 1 and various θ).

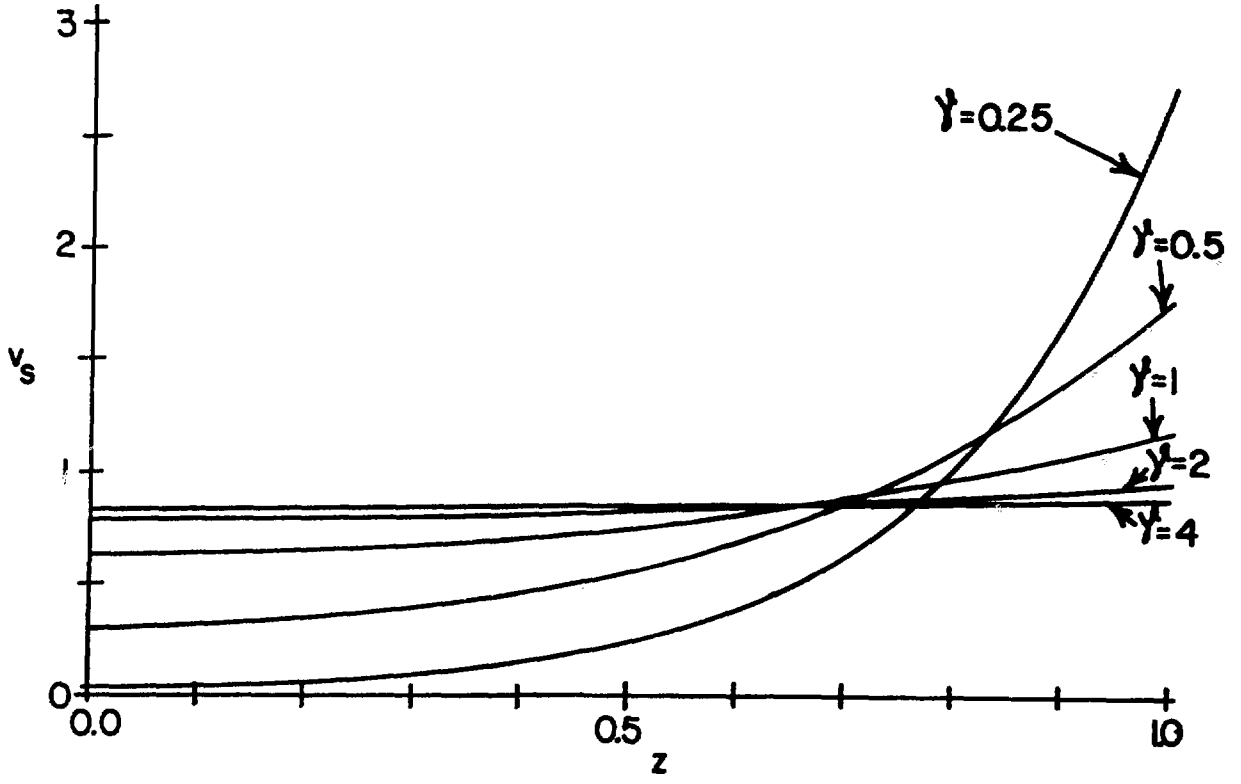

FIGURE 4c. THE CORE VELOCITY V_s PARALLEL TO THE TOP AND BOTTOM FOR $a = \beta = 1$. ($\theta = 60°$ and various γ).

increase from zero at X = 0 to maximum values at $X = X_e$. In the transition region near X_e, the circuit for the $O(c^{1/2})$ axial electric currents is completed through the core and the pressure throughout the core rises to equal $P(X_e)$. The pressure drop along the sides through the transition region is O(c) which is negligible because p and P represent the $O(c^{1/2})$ pressure.

From the design point of view, the most important result of the three-dimensional electric current circulation in the elbow is the overall pressure drop. In particular, we define the three-dimensional pressure drop as the difference between the total pressure drop and the pressure drop that would occur for locally fully developed flow, i.e., without any three-dimensional effects. For the general elbow treated in SS 2 and 3, the X derivative of the $O(c^{1/2})$ pressure P_{fd} for locally fully developed flow is

$$P'_{fd} = -2\,a\,G\,D^{-2}\,[G^{1/2} + \frac{D}{6\beta}]^{-1}$$

In terms of the dimensional pressure, the three-dimensional pressure drop is

$$\Delta p_{3D} = K\,c^{1/2}\,\sigma\,U_o\,B_o^{\,2}\,L$$

where $K = P_{fd}(X_e) - P(X_e)$ and $P_{fd}(0) = P(0)$, because the flow is fully developed at X = 0.

The values of K for $0 \le \theta \le 85°$, for $\gamma = 0.25$, 0.5 and 1.0, and for $\beta = 1$ and 5 are presented in Figure 5. As the radius of curvature decreases for a given θ_e, the value of K increases. As β increases, the value of K increases. For a 90° elbow from $\theta = \theta_e - 90°$ to $\theta = \theta_e$, we simply add the two K values for θ_e and $90° - \theta_e$.

5. CONCLUSIONS

For fully developed flows in ducts with thin metal walls, the electric field in the -z direction, $E_z = -d\phi/dz$, nearly cancels the induced electric field in the +z direction, $\hat{z}\cdot(\underline{v} \times \underline{B}) = uB_y$. The small difference drives a small O(c) j_z in the liquid metal and the electric circuit for this current is completed through the walls. A transition from one upstream fully developed flow to a different downstream fully developed flow generally involves a change in uB_y. In a non-uniform magnetic field B_y changes[8]; in a symmetric expansion or contraction, u changes because the cross sectional area changes [2]; in the present elbow, u changes because the flow turns to become nearly parallel to B. If the

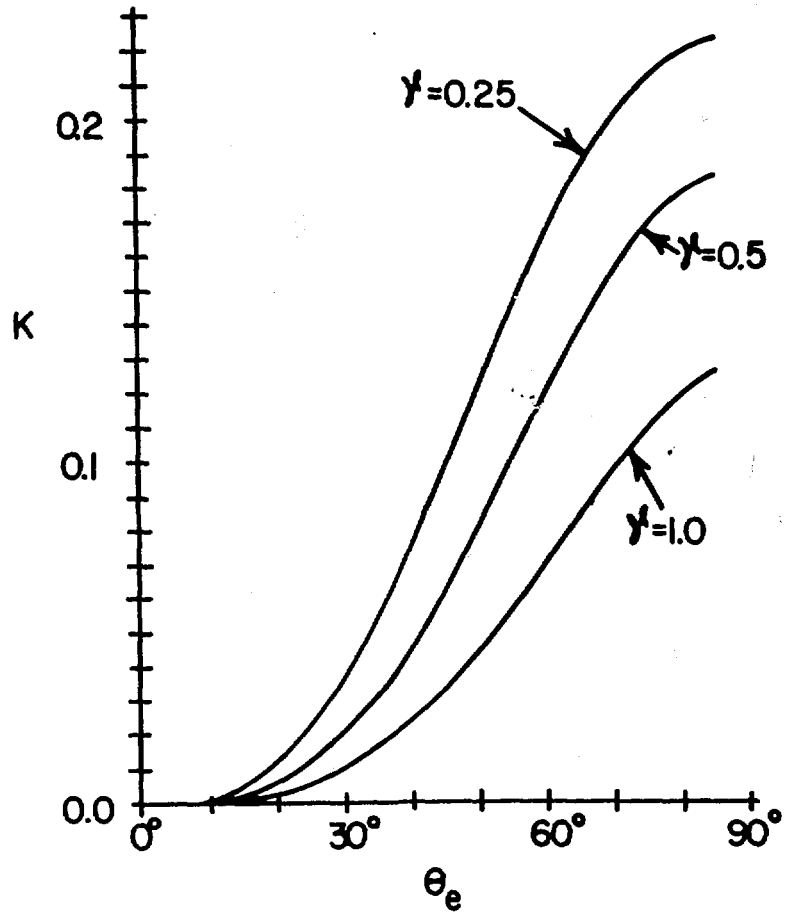

FIGURE 5a. THREE DIMENSIONAL PRESSURE DROP COEFFICIENT FOR a = 1 AND VARIOUS γ; β = 1.

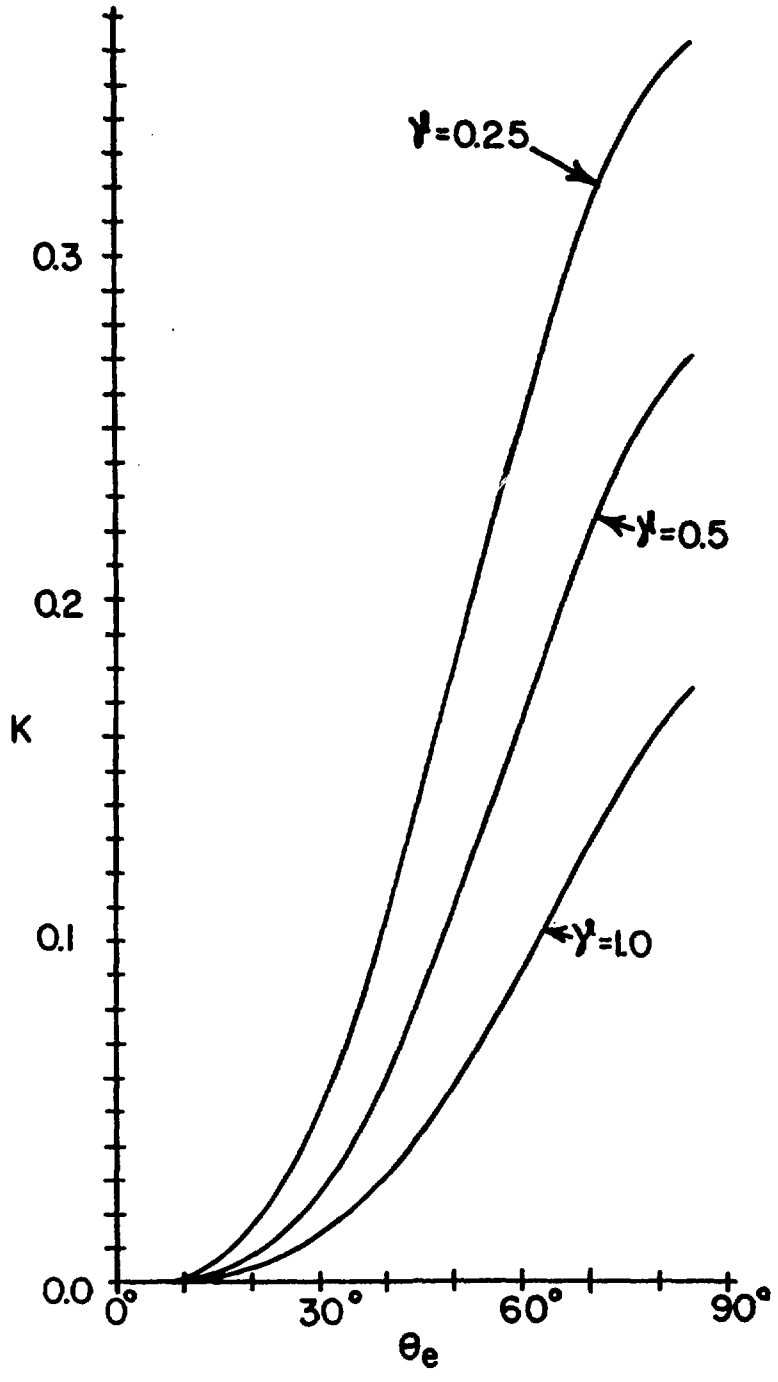

FIGURE 5b. THREE DIMENSIONAL PRESSURE DROP COEFFICIENT FOR a = 1 AND VARIOUS γ; β = 5.

values of uB_y are different in the upstream and downstream fully developed flows, then the values of $d\phi/dz$ are different, while $\phi = 0$ at $z = 0$ in both, so that there are axial potential differences for all $z \neq 0$. In the present elbow, the core potential changes from $z\ (1 + a/6\beta)^{-1}$ upstream to $z\ (1 + a/6\beta)^{-1}\cos\theta_e$ downstream. These axial potential variations drive electric currents in the $\pm x$ direction for $z \gtrless 0$, respectively. The walls are part of the electric circuit for fully developed flow. Since the walls have a high relative resistance, the electric current and the MHD pressure drop are relatively small. Once two different fully developed flows are connected, there exists an electric circuit entirely within the relatively low resistance liquid metal. The three-dimensional electric current circulations in the liquid metal and the associated three-dimensional pressures can be much larger than those in fully developed flow. The axial potential differences depend only on the two different fully developed flows, i.e., on θ_e for the present elbow. The resistance to axial currents increases as the duct length between the two fully developed flows increases, i.e., as L_{3D}/L or R_o increases. In Figure 5, as θ_e increases, the overall axial potential difference increases, so that K increases. As $\gamma = R_o c^{1/2}$ increases, the duct length between the two fully developed flows increases, so that K decreases. As β increases, the axial currents have an additional, parallel path through the thicker metal sides, so K increases.

The relationship between the three-dimensional electric current circulation due to the axial voltage differences and the three-dimensional flow disturbance is more subtle. It is wrong to say that the transverse body force associated with the axial currents pushes the flow away from the centerplane $z = 0$ and toward the sides at $z = \pm 1$. This error is immediately revealed by considering flow in the $-x$ direction in the present elbow. For this reversed flow, the transverse body forces all push away from $z = \pm 1$ and toward $z = 0$, but the flow still becomes concentrated near $z = \pm 1$.

Electric current flows in a liquid metal with a strong magnetic field are quite different from those in a solid conductor. In a solid conductor, the body force due to any current is balanced by the stress field, up to the yield strength. In a liquid metal in a strong magnetic field, the electromagnetic body force must be balanced by the pressure gradient if inertial and viscous effects are negligible, i.e., if M and N are sufficiently large. Therefore the current is constrained by the condition that $\underset{\sim}{\nabla} \times (\underset{\sim}{j} \times \underset{\sim}{B}) = 0$. With $\underset{\sim}{j}$ constrained by the momentum equation (1a), Ohm's law (1b) implies a constraint on the velocity as well. If there is a flow $\underset{\sim}{v}$ and a potential ϕ, such that Ohm's law gives an electric current $\underset{\sim}{j}$ which produces a body force $\underset{\sim}{j} \times \underset{\sim}{B}$ that cannot be balanced by a

pressure gradient ∇p, then the unbalanced, rotational part of $\underset{\sim}{j} \times \underset{\sim}{B}$ will produce accelerations of the fluid $\partial \underset{\sim}{v}/\partial \tau$, where τ is dimensionless time. These accelerations change $\underset{\sim}{v}$ until Ohm's law gives a $\underset{\sim}{j}$ whose body force can be balanced by ∇p and a steady state is reached. The dimensionless time for this adjustment is very short, namely $O(N^{-1})$. Of course all the variables are coupled and all would change during this hypothetical transient in order to approach the steady-state solution (6) satisfying the equations (1) without the inertial and viscous terms and satisfying the boundary conditions (2,5).

For a uniform magnetic field, the constraint on $\underset{\sim}{j}$ from the momentum equation is that $\underset{\sim}{j}$ must be independent of y. At a given X and $\underset{\sim}{z}$ in the present elbow, there is a specific axial current which is parallel to the top and bottom, as reflected in the equation (6b), and is uniform in y. As this axial current progresses from X to X + ΔX, the distance between the top and bottom increases because $D' > 0$. However the current lines for the axial current in the core cannot be spread to accommodate this expansion because j is independent of y. The currents needed in the additional parts of the cross section must come from the top and bottom and exactly the right current must flow out of each wall to give the new current distribution at X + ΔX which is again uniform in y. Through the boundary conditions (2), this relates ϕ to the axial currents and D'. Then Ohm's law determines u, as in equation (6d).

We have not considered an elbow with $\theta_e = 90°$. For the present downstream duct with $\theta_e < 90°$, the axial pressure gradient for fully developed flow is

$$\frac{\partial p}{\partial s} = - A\, c\, \sigma\, U_o\, B_o^2 \cos^2 \theta_e \tag{19}$$

For a duct which is parallel to the uniform magnetic field, the flow is ordinary, laminar, Poiseuille flow with

$$\frac{\partial p}{\partial s} = - \frac{f \rho U_o^2}{2 D_h} \tag{20}$$

where f and D_h are the friction factor and hydraulic diameter, respectively. This pressure gradient is much smaller than that given by the equation (19) for $\theta_e = 85°$, so that one might try to align the ducts with the magnetic field in order to decrease the pressure gradient. However, the formula (20) assumes that the Hartmann number based

on the transverse magnetic field strength $B_o \cos \theta_e$ is small, i.e., that

$$\cos \theta_e << M^{-1}$$

With $M = 10^3 - 10^5$, it is impossible to make the duct so perfectly parallel to the magnetic field, especially for a variety of operating conditions. Therefore, the parallel field case with the small pressure gradient (20) represents a very singular limit which cannot be realistically expected in any blanket design. The limits of the present analysis are indicated by the conditions (14) with N and M based on $B_o \cos \theta_e$.

REFERENCES

[1] Walker, J. S., "Laminar Duct Flows in Strong Magnetic Fields (Single- and Multi-Phase Flows in an Electromagnetic Field, Energy, Metallurgical and Solar Applications," Ed. by H. Branover, P. S. Lykoudis and M. Mond, Progress in Astronautics and Aeronautics, Vol. 100, American Institute of Aeronautics and Astronautics, New York, 1985, pp. 3-16.

[2] Walker, J. S., "Magnetohydrodynamic Flows in Rectangular Ducts with Thin Conducting Walls. Part 1, Constant-Area and Variable Area Ducts with Strong Magnetic Fields," J. Mecanique, Vol. 20, 1981, pp. 79-112.

[3] Walker, J. S., "Liquid Metal MHD Flow Through a Thin Walled Elbow in a Plane Perpendicular to a Uniform Magnetic Field," Int. J. Engng. Sci., Vol. 24, 1986, pp. 1741-1754.

[4] Walker, J. S., "Liquid Metal MHD Flow in a Duct Whose Corss Section Changes from a Rectangle to a Trapezoid," Int. J. Engng. Sci., Vol. 25, 1987, pp. 351-371.

[5] Smith, D. L. et. al, "Blanket Comparison and Selection Study - Final Report," Argonne National Laboratory Report ANL-FPP-84-1, 1984.

[6] Holroyd, R. J. and Walker, J. S., "A Theoretical Study of the Effects of Wall Conductivity, Non-Uniform Magnetic Field and Variable-Area Ducts on Liquid Metal Flows at High Hartmann Number," J. Fluid Mech., Vol. 84, 1978, pp. 471-495.

[7] Talmage, G. and Walker, J. S., "Three Dimensional Laminar MHD Flows in Ducts with Thin Metal Walls and Strong Magnetic Fields," Proceedings of the 6th Beer Sheva Semiar, March 1987.

[8] Walker, J. S., "Liquid Metal Flow in a Rectangular Duct with a Non-Uniform Magnetic Field," J. Mecan. Theor. et Appl., Vol. 5, 1987, pp 827-851.

[9] Walker, J. S. Ludford, G. S. S., and Hunt, J. C. R., "Three-Dimensional MHD Duct Flows with Strong Transverse Magnetic Fields, Part 3, Variable-Area Rectangular Ducts with Insulating Walls," J. Fluid Mech., Vol. 56, 1972, pp. 121-141.

[10] Walker, J. S., "Liquid Metal Flow in a Rectangular Duct with a Non-uniform Magnetic Field," Argonne National Laboratory Technical Memo, ANL/FPP/TM-207, 1986.

DISTRIBUTION FOR ANL/FPP/TM-227

Internal:

H. Attaya
C. Baker
E. Bennett
M. Billone
J. Brooks
Y. Cha
O. Chopra
R. Clemmer
D. Ehst
K. Evans
P. Finn
Y. Gohar
L. Greenwood
D. Gruen
A. Hassabein
T. Hua
A. Hull
C. Johnson
A. Krauss
Y. Liu
B. Loomis
S. Majumdar
R. Mattas
B. Picologlou
R. B. Poeppel
K. Porges
C. Reed
D. Smith
H. Stevens
D. Sze
L. Turner
T. Yule
FPP Files (25)
ANL Contract File
ANL Libraries
ANL Patent Dept.
TIS Files (3)

External:

DOE-OSTI for Distribution per UC-420 (37)
Manager, Chicago Operations Office
M. Abdou, University of California - Los Angeles
J. Anderson, Los Alamos National Laboratory
L. Barleon, KfK, Germany
J. Barlit, Los Alamos National Laboratory
W. Bauer, Sandia Laboratories
S. Berk, Office of Fusion Energy
L. Bromberg, Massachusetts Institute of Technology
J. Clarke, Office of Fusion Energy
M. Cohen, Office of Fusion Energy
D. Cohn, Massachusetts Institute of Technology
R. Conn, University of California - Los Angeles
J. Crocker, EG&G Idaho, Inc.
J. Davis, McDonnell Douglas Astronautics Company
S. Dean, Fusion Power Associates
R. Dowling, Office of Fusion Energy
P. Dunn, University of Notre Dame
C. Flanagan, Oak Ridge National Laboratory
H. Forsen, Bechtel National Inc.
H. Furth, Priceton Plasma Physics Laboratory
P. Gierszewski, Canadian Fusion Fuels Technology Project
J. Gordon, TRW, Inc.
R. A. Gross, Columbia University
G. Haas, Office of Fusion Energy
R. Hancox, Culham Laboratory
C. Henning, Lawrence Livermore National Laboratory
D. Holland, EG&G Idaho, Inc.
N. Hoffman, Energy Technology Engineering Center
G. Hollenberg, Hanford Engineering Development Laboratory
M. Hsiao, Pennsylvania State University

J. Hunt, Cambridge University, UK
M. Krazimi, Massachusetts Institute of Technology
A. Klein, University of Oregon
R. Krakowski, Los Alamos National Laboratory
G. Kulcinski, Univeristy of Wisconsin - Madison
R. Little, Princeton University
B. Logan, Lawrence Livermore National Laboratory
P. Lykoudis, Purdue University
H. Madarame, University of Tokyo, Japan
J. Maniscalco, TRW, Inc.
G. Miley, University of Illinois - Champaign-Urbana
K. Miya, University of Tokyo, Japan
K. Miyazaki, Osaka University, Japan
R. Moir, Lawrence Livermore National Laboratory
B. Montgomery, Massachusetts Institute of Technology
D. Moyer, Grumman Aerospace Corporation
Prof. U. Muller, KfK, Germany
G. R. Nardella, Office of Fusion Energy (2)
Yuji Naruse, Japan Atomic Energy Research Institute
A. Opdenaker, Office of Fusion Energy
S. Piet, EG&G Idaho
J. Ramos, Carnegie Melon University
T. Reuther, Office of Fusion Energy
F. Ribe, University of Washington
M. Rogers, Monsanto Research Corporation
P. Rutherford, Princeton Plasma Physics Laboratory
J. Schmidt, Princeton Plasma Physics Laboratory
K. Schultz, GA Technologies, Inc.
T. Shannon, Oak Ridge National Laboratory
M. Snykers, MOL, Belgium
W. M. Stacey, Georgia Institute of Technology
D. Steiner, Rensselaer Polytechnic Institute
P. Stone, Office of Fusion Energy
K. Thomassen, Lawrence Livermore National Laboratory
A. Tobin, Grumman Aerospsace Corporation
T. Tomabechi, Japan Atomic Energy Research Institute, Japan
W. Verbeeck, CEC, Belgium
Prof. Better, Kenrforschungszentrum Karlsruhe und Verwaltung, Germany
J. Walker, University of Illinois-Champaign-Urbana (12)
G. L. Woodruff, University of Washington
H. Yoshida, Los Alamos National Laboraotry
Bibliothak, Max-Planck-Institute fur Plasmaphysik, West Germany
C.E.A. Library, Fontenay-aux-Roses, France
Librarian, Culham Laboratory, England
Library, Laboratorio Gas Ionizati, Italy
Thermonuclear Library, Japan Atomic Energy Research Institute, Japan